A theoretical DFT investigation of the lysozyme mechanism: Computational evidence for a covalent intermediate pathway

ARTICLE *in* PROTEINS STRUCTURE FUNCTION AND BIOINFORMATICS · APRIL 2005

Impact Factor: 2.63 · DOI: 10.1002/prot.20396 · Source: PubMed

3 AUTHORS:

Andrea Bottoni
University of Bologna
147 PUBLICATIONS **2,418** CITATIONS
SEE PROFILE

Gian Pietro Miscione
University of Bologna
33 PUBLICATIONS **628** CITATIONS
SEE PROFILE

Marco De Vivo
Istituto Italiano di Tecnologia
43 PUBLICATIONS **711** CITATIONS
SEE PROFILE

A Theoretical DFT Investigation of the Lysozyme Mechanism: Computational Evidence for a Covalent Intermediate Pathway

Andrea Bottoni,[1*] Gian Pietro Miscione,[1*] and Marco De Vivo[2]
[1]*Dipartimento di Chimica "G.Ciamician," Universita' di Bologna, Bologna, Italy*
[2]*University of Pennsylvania, Department of Chemistry, Philadelphia, Pennsylvania*

ABSTRACT **A theoretical DFT(B3LYP) investigation of the catalytic cycle of lysozyme has provided further evidence for a mechanism involving a glycosil-enzyme covalent intermediate, in agreement with recent experimental data. This type of intermediate has been located along two different pathways. Along the favored path the retention of the anomeric configuration of the peptidoglycan NAM unit involved in the reaction, is the result of two subsequent inversions at the C_1 carbon. The other path involves the opening of the pyranose ring and a nucleophilic attack on the prochiral carbonyl group of the open aldehyde, restoring the original anomeric configuration. No evidence has been found for a pathway characterized by the formation of an oxocarbenium ion (stabilized by resonance and electrostatic interactions), as suggested in the most popular mechanistic schemes. Proteins 2005; 59:118–130.** © 2005 Wiley-Liss, Inc.

Key words: lysozyme; glycosidase; enzyme mechanism; DFT investigation

INTRODUCTION

Lysozyme, discovered by Fleming in 1922, belongs to a large class of enzymes known as glycosidases.[1–4] These enzymes are extremely efficient catalysts, capable of hydrolyzing the glycosidic bond, which is the most stable of the linkages occurring in natural biopolymers. While the half-lives for spontaneous hydrolysis of cellulose and starch are in the range of five millions of years, glycosidases can accomplish this hydrolysis with rate constants up to 1000 s^{-1}. Glycosidases can be separated into two major classes: those hydrolyzing the glycosidic bond with net inversion of the anomeric configuration and those doing this task with net retention. Animal or C-type lysozymes belong to the latter of these classes and selectively cleave the glycosidic linkage between the anomeric carbon C_1 of N-acetylmuramic acid (NAM) and the oxygen at the C_4 carbon of N-acetylglucosamine (NAG) of peptidoglycan, the polysaccharide component of bacterial cell walls.[5–8] The process occurs with net retention of configuration at C_1. The best characterized C-type lysozyme in structural and mechanistic studies is that isolated from hen egg-white (HEWL).[8–30] HEWL was also the first enzyme to have its three-dimensional structure determined by X-ray diffraction techniques.[13–17] This enzyme is rather small (it comprises only 129 amino acid residues) and is characterized by a deep crevice that contains the substrate binding site and divides the molecule into two domains: one has almost entirely a β-sheet structure and the other is most helical in nature. Six sugar units (termed A through F) of the polysaccharide substrate can be accommodated within the enzyme active-site cleft. The cleavage of the glycosidic bond occurs between unit D and E (see Scheme 1).

Over the last three decades two main mechanistic schemes have been proposed for the lysozyme action. One of them supposes the existence of a long-lived oxocarbenium-ion intermediate and was suggested by Phillips and coworkers.[17] This mechanistic hypothesis has been considered for a long time as the paradigm of the mechanisms of the β-glycosidases, which cleave the glycosidic bonds with net retention of configuration. In this mechanism (see Scheme 2, mechanism 1) the substrate (polysaccharide) is bound by the enzyme in the active-site-cleft and the two residues Glu35 (protonated) and Asp52 (ionized) embody the glycosidic oxygen that links the NAM and NAG units at site D and E, respectively. Glu35 acts as a general acid catalyst and donates a proton to the glycosidic oxygen. This causes the cleavage of the glycosidic bond and the formation of a positively charged intermediate (oxocarbenium ion). The positive charge on this ion (and thus the transition state for the exocyclicic C-O bond cleavage) is stabilized by the lone-pair of the NAM ring oxygen and by the interaction with the negative carboxylate group of the Asp52 residue. It has been observed that an essential feature of this mechanism is the distortion of the ring at site D. This residue assumes a twist-boat conformation that makes possible a better stabilization of the transition state. A water molecule (nucleophile) attacks the NAM unit at C_1 on the only accessible face of the oxocarbenium ion (on the opposite side with respect to Asp52, which shields the β-face), thus retaining the anomeric configuration. A final transfer of a proton from water to Glu35 completes the catalytic cycle.

The Supplementary Materials referred to in this article can be found at http://www.interscience.wiley.com/jpages/0887-3585/suppmat/index.html

*Correspondence to: Andrea Bottoni or Gian Pietro Miscione, Dipartimento di Chimica "G.Ciamician," Universita' di Bologna, via Selmi 2, 40126 Bologna, Italy. E-mail: andrea.bottoni@unibo.it

Received 4 June 2004; Accepted 1 October 2004

Published online 1 February 2005 in Wiley InterScience (www.interscience.wiley.com). DOI: 10.1002/prot.20396

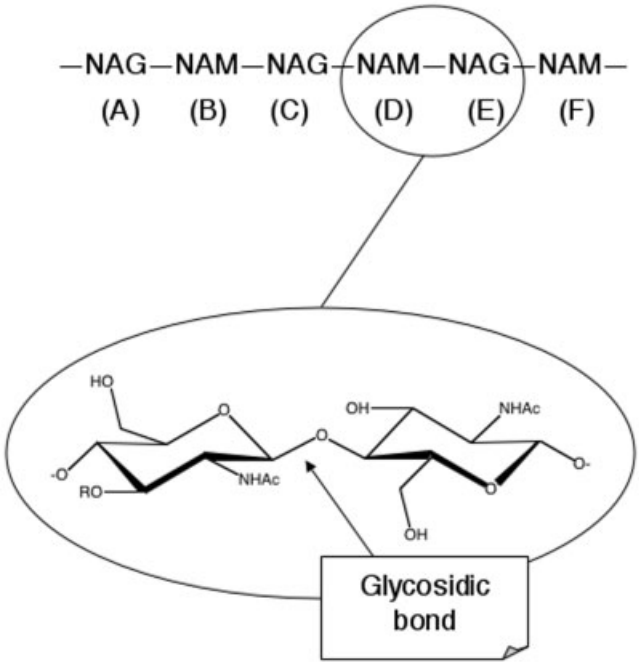

Scheme 1

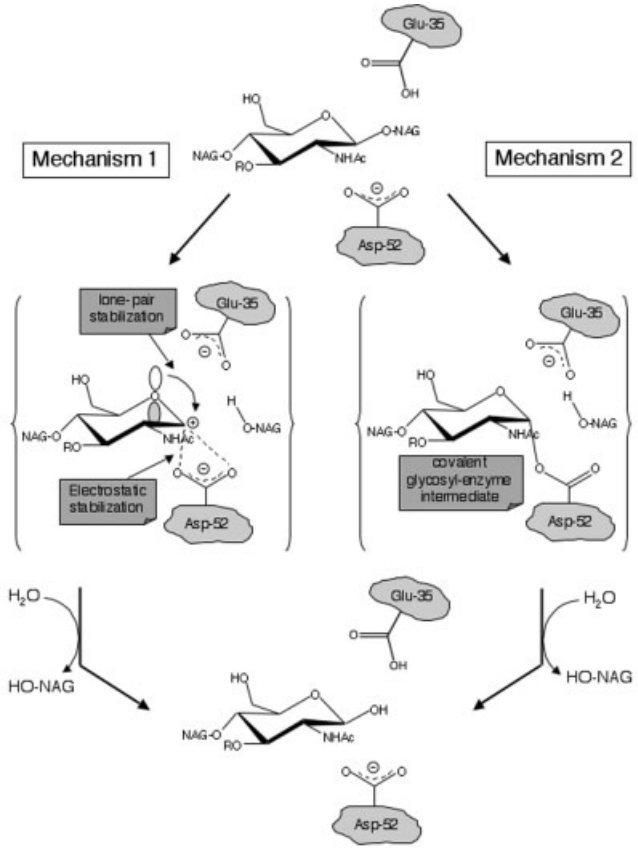

Scheme 2

The alternative mechanism[25,26,28] (mechanism 2 in Scheme 2) involves the formation of a glycosyl-enzyme intermediate originated by the nucleophilic attack of the Asp52 carboxylate group in a concerted S_N2-type reaction, causing the inversion of configuration at the C_1 center. In a subsequent step the Asp52 carboxylate is displaced by a water molecule, with a second inversion, which restores the original anomeric configuration.

The major criticism[28,29] to the first mechanistic scheme concerns the nature and stability of the ion-pair intermediate. The glicosyl cation is characterized in water by a very short life-time, about 10^{-12} sec, which is much shorter than the time required for diffusion events. Thus, such a cation and, consequently, the supposed ion-pair in mechanism 1 would not exist long enough to play an active role in the catalysis. Things are expected to be different for the glycosil-enzyme intermediate proposed in mechanism 2, an acyl glycoside that should be relatively stable in solution. However, in spite of this supposed stability, the glycosil-enzyme intermediate has never been observed in the reactions of the wild-type enzyme. Thus the mechanistic scenario for the catalytic action of lysozyme has remained quite confused and the nature of the intermediate a point of contention.

Very recently Vocadlo and coworkers[27] gave for the first time a convincing evidence for the existence of such an intermediate along the lysozyme reaction pathway. These authors introduced in the enzyme active site a mutation, to slow down the reaction and increase the intermediate life-time. In this way the concentration of the intermediate in the mutant lysozyme was high enough to be detected by electrospray ionization mass spectrometry. Also, using a doubly fluorinated substrate (in position C_1 and C_2 of the NAM unit) they obtained a glycosil-enzyme intermediate living long enough for determining the corresponding crystal structure.

While a large number of experimental investigations on lysozyme structure and its action mechanism are available in literature, the problem has not been carefully investigated at a theoretical level. Warshel and Levitt[31] in 1976 studied the mechanism of lysozyme using a QM-MM approach. These authors examined the stability of the carbenium ion intermediate that is supposed to form after the cleavage of the glycosidic bond. They found that electrostatic stabilization is an important factor in increasing the rate of the catalytic step leading to the intermediate formation, while steric factors do not give a significant contribution. Ten years later Post and Karplus[32] carried out a molecular dynamics simulation of a complex of lysozyme with the N-acetylglucosamine hexamer. The results of the simulation suggested a new pathway where an endocyclic bond is broken in the initial step of the reaction. This mechanism (mechanism 3), which does not require the ring distortion described in mechanism 1, is schematically represented in Scheme 3. The initial step is the protonation of the ring oxygen by Glu35. The cleavage of the endocyclic C_1-O bond leads to a noncyclic oxocarbenium ion intermediate stabilized by the Asp52 residue. The subsequent attack of a water molecule determines the

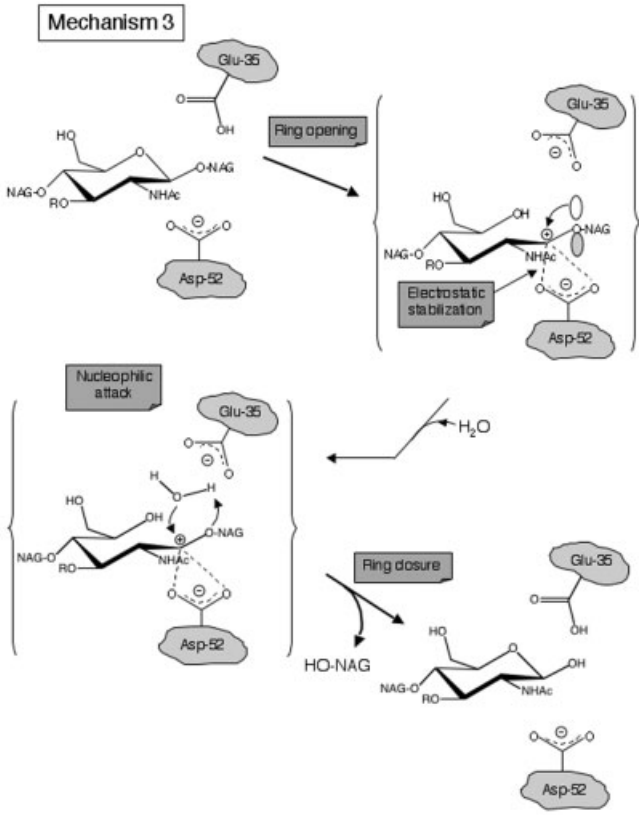

Scheme 3

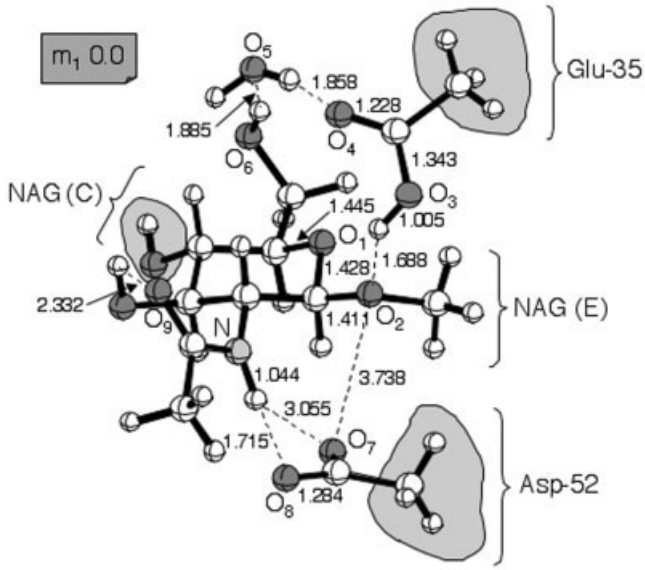

Fig. 1. A schematic representation of the critical point m_1 (starting Michaelis complex) illustrating the model-system used in this paper (bond lengths are in angstroms). The contour lines mark the groups that are kept frozen during the geometry optimization.

expulsion of the HO-NAG fragment. The ring closure leads to the final product.

More recently Karplus and coworkers found evidence for an oxocarbenium ion intermediate in the case of the uracil-DNA glycosylase UDG. For this particular glycosylase these authors carried out a theoretical investigation of the catalytic mechanism and found that a specific enzyme-substrate interaction contributes to lower the energy of the rate-determining transition state and stabilizes the oxocarbenium cation.[33]

Since, to our knowledge, no further investigations at a theoretical level are available in literature and many mechanistic aspects have not been elucidated yet, we have carried out a computational DFT investigation of the catalytic mechanism of lysozyme. The results are reported in the present paper where we examine the three possible mechanisms described above and we try to answer the following questions: (i) Do all three reaction channels, corresponding to mechanism 1, 2 and 3, exist on the potential energy surface? (ii) Is the formation of a covalent intermediate evident at a computational level? (iii) Is there any indication for the existence of an energetically accessible oxocarbenium cation intermediate? (iv) What is the rate-determining step of the catalytic process? (v) Do the proton transfer from the Glu-35 residue and the breaking of the glycosidic bond occur simultaneously or in two subsequent kinetic steps? (vi) What are the nature and the importance of the hydrogen bond network between the substrate and the protein residues? In the present study, to try to elucidate all these points, we use a model-system that includes the Glu35 and Asp52 residues, a water molecule and a β-methyl-N-acetylglucoside emulating the NAM unit at position D of the natural polysaccharide substrate.

COMPUTATIONAL DETAILS AND CHOICE OF THE MODEL

The model-system used here to emulate the lysozyme active site and explore the reaction potential surface (see Fig. 1), has been assembled using the crystallographic structure available in literature (protein data bank code is 193L, 1.33-Å resolution).[29] This system includes: (i) the Asp52 and Glu35 residues; (ii) a water molecule; (iii) a substrate molecule. To reduce the size of the model-system an acetate molecule and an acetic acid molecule have been used to emulate the Asp52 and the Glu35 residues, respectively. A six-membered β-methylglucoside with an acetamido group bonded at the C_2 carbon has been used as a substrate. This glucopyranose ring mimics the NAM unit at position D while the methyl group emulates the NAG unit at the subsequent position E.

To preserve the geometry of the active-site cavity and thus emulate the partially constraining effect of the protein environment, during the geometry optimization procedure we have fixed the positions of the atoms not directly involved in the reaction or in the formation of hydrogen bonds. These atoms are marked by contour lines in Figure 1. The methyl carbons of the Glu-35 and Asp-52 residues have been anchored to their crystallographic coordinates and one hydrogen atom of each methyl group has been maintained along the direction of the protein backbone. In addition, the OH group bonded at C_4 has been frozen in the position obtained from PM3 computations where a larger

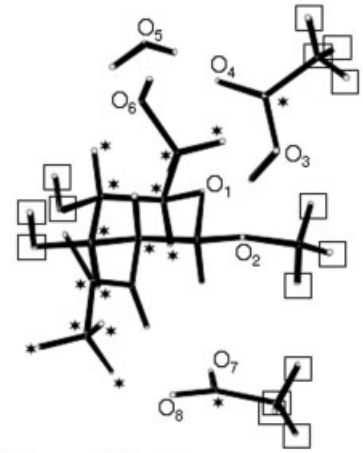

Scheme 4

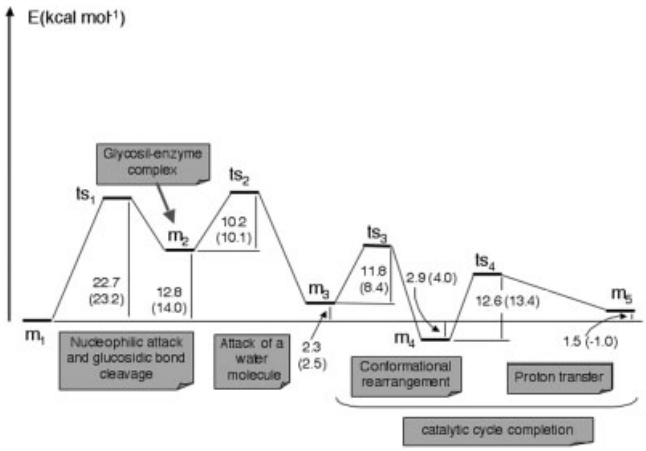

Fig. 2. Energy profiles obtained for the various steps of mechanism 2. The values in parenthesis are obtained with the solvent COSMO model.

model-substrate formed by the NAM and NAG units at position D and E, respectively, has been fully relaxed within the active site. The protonation state of the Glu35 residue and the position of the water molecule correspond to the lowest energy arrangement obtained at the DFT level. This method has been used to explore the whole potential surfaces corresponding to the various mechanistic hypothesis.

All the reported DFT computations have been carried out with the Gaussian 98 series of programs[34] using the B3LYP[35] functional that has been demonstrated to be suitable for systems involving hydrogen bond interactions[36–42] and to provide a satisfactory description of enzymatic reactivity.[42,43] A locally dense basis set (LDBS)[44] approach has been adopted. According to this method, the system has been partitioned into three different regions, which were assigned basis sets of different accuracy. The assignment is indicated in Scheme 4. The atoms contained in the squares are described by the minimal STO-3G basis[34] and those marked by an asterisk by the 3-21G basis.[34] For all the remaining atoms (i.e. the atoms directly involved in the reaction or in the formation of hydrogen bonds) the DZVP[46] basis has been chosen. This basis, which is a Local Spin Density (LSD)-optimized basis set of double-zeta quality and includes polarization functions, is suitable to describe hydrogen interactions such as those occurring in the system investigated here. The transition vector of the various transition states has been analyzed by means of frequency computations. Furthermore, to validate the DFT results, the energy of some important critical points have been recomputed at the MP2 level.

The effect of the whole protein environment has been evaluated with the solvent continuous model approach COSMO[48] as implemented in the Turbomole package.[50] Single-point computations have been performed on the DFT-optimized structures using the dielectric constant of nitromethane (ϵ = 38.2). It has been demonstrated that the solvation energies obtained from single-point PCM calculations using gas-phase DFT structures are in satisfactory agreement with the values obtained after geometry optimization in the presence of solvent effects.[51,52] The value of 38.2 for the dielectric constant has been chosen to take into account the simultaneous presence of hydrophilic and hydrophobic groups around the active site. A value of about 40 has been suggested elsewhere to take into account the effect of charge–charge interactions in proteins.[53] Several papers are available in the literature where the COSMO approach has been used in calculations on enzymatic models involving hydrogen bonds and proton transfer.[41–43,54]

RESULTS AND DISCUSSION

In this section we examine in detail the singlet potential energy surfaces that we have obtained in the investigation of the mechanistic hypothesis of Scheme 2 and 3. The corresponding energy profiles are reported in Figure 2 and Figure 7. The structures (with the corresponding energies) of the various critical points located along these profiles are schematically represented in Figures 3–6 and Figures 8–14.

Mechanisms 1 and 2: The Nucleophilic Attack and the Glucosidic Bond Cleavage

A complex network of hydrogen bonds characterizes the intermediate m_1, which forms upon insertion of the substrate in the enzyme active site (Michaelis complex, see Fig. 1). A fairly strong hydrogen bond engages the glutamate hydrogen and the glycosidic oxygen O_2. This interaction is characterized by a short O_2…H-O_3 distance (1.688 Å) and prepares the proton transfer from O_3 to O_2, as postulated in both mechanisms 1 and 2. The water molecule is kept in its position by two hydrogen bonds, one involving the water hydrogen and the Glu35 oxygen O_4 (O_4…H-O_5 distance = 1.858 Å) and the other the water oxygen O_5 and the OH group bonded at carbon C_6 (O_5…H-O_6 distance = 1.885 Å). Another hydrogen bond can be detected between the NH group of the acetamido

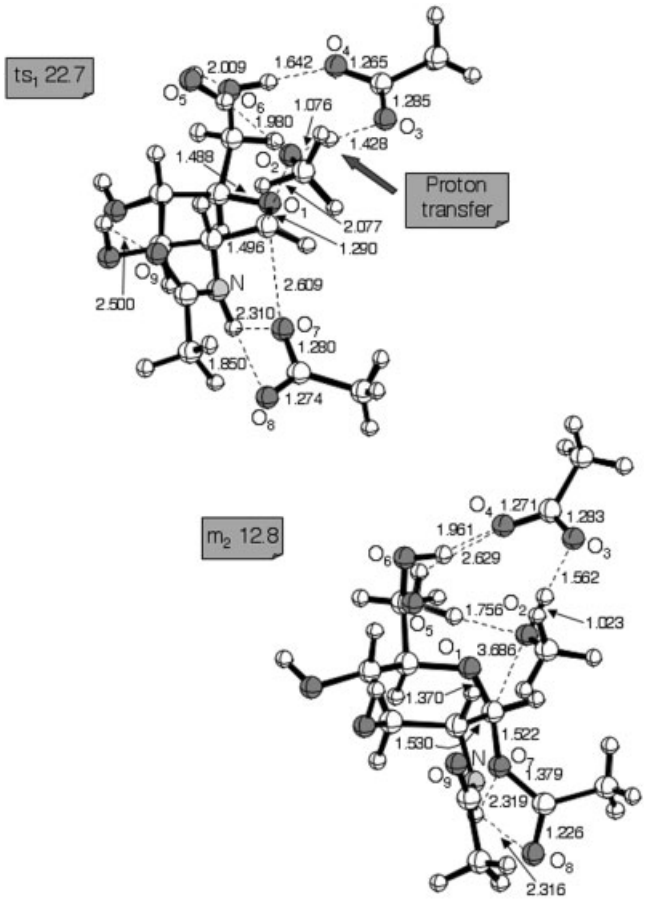

Fig. 3. Schematic representation of the structures of the critical points ts_1 and m_2 (bond lengths are in angstroms). The energy values (kcal mol^{-1}) are relative to m_1.

fragment and the oxygen atom O_8 of the aspartate residue (O_8…H-N distance = 1.715 Å). This bond determines the relative orientation of the Asp52 and $NH(CO)CH_3$ groups. The position of the acetamido group, which can rotate around the C_2-N bond, is also determined by the hydrogen bond between the carbonyl group of $NH(CO)CH_3$ and the OH bonded at C_3 (O_9…H-O_{10} = 2.332 Å).

The first step of the catalytic process, following mechanism 1 or 2, could be either concerted or not concerted. In the former case the proton transfer from O_3 to O_2 (acidic catalysis) and the breaking of the glycosidic bond with the expulsion of the methanol molecule should occur in the same kinetic step. In the latter the formation of an intermediate where the glycosidic oxygen is protonated, should be observed. A careful examination of the potential surface has demonstrated that such an intermediate does not exist, because the protonation of the O_2 oxygen immediately causes the expulsion of the methanol molecule. The search for a concerted channel has lead to transition state ts_1 (see Fig. 3) where the proton transfer and the breaking of the glycosidic bond C_1-O_2 occur simultaneously. In ts_1 the proton has been almost completely transferred from O_3 to O_2 (the H-O_2 and H-O_3 distances are 1.076 and 1.428 Å, respectively) and the breaking C_1-O_2 bond is 2.077 Å. However, the concerted character of ts_1 does not concern only the proton transfer and the expulsion of methanol. The breaking of the glycosidic linkage is accompanied by a rotation of the Asp52 residue around the C-C bond. This rotation moves the oxygen O_7 much closer to the anomeric center and the C_1-O_7 distance becomes 2.609 Å (an incipient carbon–oxygen bond). A simultaneous structural rearrangement of the ring is observed, the anomeric center being now approximately planar. Thus ts_1 resembles very closely a S_N2 transition state, characterized by a configuration inversion, where the incoming group is the Asp52 carboxylate oxygen and the leaving group is the methanol molecule. This nucleophilic attack, which has an energy barrier of 22.7 kcal mol^{-1}, is assisted by the $O_3 \rightarrow O_2$ proton transfer and by a complex network of hydrogen bonds. In particular the hydrogen bonds involving the N-H bond of the acetamido group and the two oxygen atoms of the Asp52 residue are interesting. On passing from m_1 to ts_1 the N-H…O_7 interaction becomes significantly stronger (the H…O_7 distance varies from 3.055 to 2.310 Å) and contributes to the stabilization of the transition state. In the absence of these interactions (for instance, in case of removal of the acetamido group) a higher activation barrier is certainly expected. This finding is in agreement with the suggested participation of the substrate C_2-bonded acetamido group in the catalysis.[3] This hypothesis was based on the experimental evidence obtained in the study of the hydrolysis by hen egg white lysozyme of N-acetyl-chitobioside substrates with either a C_2 hydroxyl or C_2 acetamido group. After removal of the C_2 acetamido group a reduction of about 100-fold in k_{cat} was observed. It is worth to point out that these observations agree with the hypothesis that the step involving the acetamido group is the rate-determining step of the process.

The analysis of the transition vector confirms the nature of the transition state ts_1, since the dominant components are the breaking C_1-O_2 and forming C_1-O_7 bonds and the H-O_2 and H-O_3 distances.

We move from ts_1 to the intermediate m_2, where the new C_1-O_7 bond is completed (1.522 Å). This species (schematically represented in Fig. 3) corresponds to the postulated glycosyl-enzyme intermediate of mechanism 2, where the configuration of the anomeric center C_1 is inverted. The methanol molecule is now far away from the ring, the O_2-C_1 distance being 3.686 Å. The position of this molecule within the active site is determined by two strong hydrogen bonds: one between the methanol hydrogen and the glutamate oxygen O_3 (O_3…H-O_2 distance = 1.562 Å) and the other involving the methanol oxygen and one water hydrogen (O_2…H-O_5 distance = 1.756 Å). The water molecule, in turn, is hydrogen-bonded to the glutamic oxygen O_4. Also, two additional hydrogen bonds (N-H…O_7 and N-H…O_8) fix the orientation of the $NH(CO)CH_3$ group and contribute to stabilize m_2.

We outline once again that all the attempts to locate a planar oxocarbenium intermediate (planar positively charged anomeric center stabilized by the oxygen lone-pair and the electrostatic interaction with the Asp52 residue, as postulated in mechanism 1) failed. In all cases the

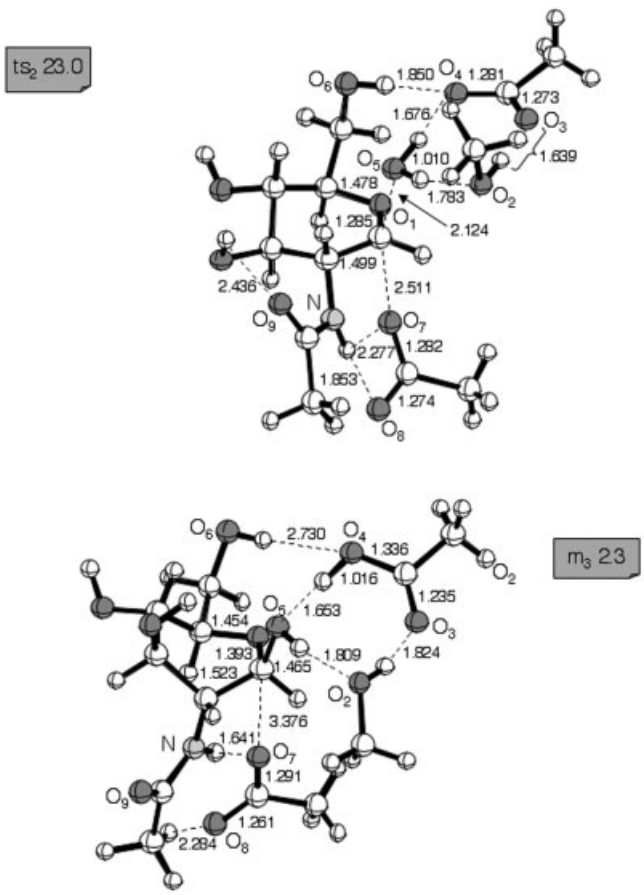

Fig. 4. Schematic representation of the structures of the critical points ts_2 and m_3 (bond lengths are in angstroms). The energy values (kcal mol^{-1}) are relative to m_1.

search algorithm collapsed to the critical point m_2, enforcing the hypothesis of mechanism 2. It is important to stress that the structural features of the lysozyme-substrate complex are significantly different from those of the glycosylase-substrate complex investigated by Karplus.[33] In that case phosphate groups of the DNA substrate provide stabilizing interactions that make possible the existence of an oxocarbenium ion intermediate. In the lysozyme the key-interaction is that between the negatively charged Asp52 residue and the incipient positive charge at the anomeric center C_1. Because of the proximity of the two charged centers a slight distortion of the system easily leads to the formation of the stabilizing carbon-oxygen bond in m_2.

Mechanisms 2: The Attack of the Water Molecule

In the second step the water molecule undergoes a nucleophilick attack on carbon C_1. This requires a barrier of 10.2 kcal mol^{-1} (transition state ts_2) and causes a second configuration inversion, thus restoring the original configuration of the anomeric center. The structure of ts_2 (see Fig. 4) is similar to that of ts_1. The anomeric carbon is again approximately planar (as expected in a S_N2-type transition state), the breaking C_1-O_7 and forming C_1-O_5 bonds are 2.551 and 2.124 Å (2.609 and 2.077 Å in ts_1, respectively) and the orientation of the glutamate residue and acetamido group is almost identical to that described in ts_1. It is interesting to note that the two hydrogen bonds N-H…O_7 and N-H…O_8 are again important in stabilizing the transition state since they become stronger on passing from m_2 to ts_2, as evidenced by the H…O_7 and H…O_8 distances.

Among the most important components of the transition vector obtained from frequency computation there are, as expected, the C_1-O_7 and C_1-O_5 bonds, i.e., the two bonds involved in the S_N2-like process. However important contributions are also associated with the H…O_4 and H…O_5 distances, indicating that a proton transfer simultaneously occurs from the water oxygen O_5 to the glutamate oxygen O_4. This transfer process is at the beginning since only a slight lengthening of the H…O_5 bond (1.010 Å) is observed. However, the hydrogen strongly interacts with the O_4 oxygen (H…O_4 distance = 1.676 Å) and this interaction probably contributes to further stabilize ts_2 and certainly increases the nucleophilic character of the water oxygen. Both these factors contribute to make the corresponding activation barrier much lower than that found for ts_1. The transition state ts_2 results in the formation of the intermediate m_3 (Fig. 4), which is only 2.3 kcal mol^{-1} higher than m_1. Here the new C_1-O_5 bond is completed (1.465 Å) and the O_7-C_1 bond definitely broken (the O_7-C_1 distance is 3.376 Å). The proton transfer from the water molecule to the glutamate residue Glu-35 is also achieved, so the original protonation of this residue is restored. Three hydrogen bonds (O_4-H…O_5, O_5-H…O_2 and O_2-H…O_3) involve the OH group bonded to the anomeric center, the Glu-35 residue and the expelled methanol molecule and are arranged to form a cyclic structure. Another interesting structural feature of m_3 is the following: after the breaking of the C_1-aspartate linkage, the pyranose ring has not recovered yet the original chair form found in m_1, but is now characterized by a distorted boat conformation.

Mechanism 2: The Catalytic Cycle Completion

It is evident that, to restore the starting situation of the enzyme (m_1 complex) a conformational rearrangement of the ring is needed. We have located a transition state ts_3 (see Fig. 5) connecting the complex m_3 to a new intermediate m_4 (2.9 kcal mol^{-1} lower than m_1) where the substrate has completely recovered the more stable chair conformation. In ts_3 the anomeric center is planar, the dihedral angle $O_1C_1C_2C_3$ being 0.3°. The ring distortion required by the boat → chair transformation does not modify significantly the stabilizing network of hydrogen bonds that characterizes the preceding critical point so that the resulting energy barrier is only 11.8 kcal mol^{-1}. Also, two hydrogen bonds (O_6-H…O_4 and O_5-H…O_4) become stronger on passing from m_3 to ts_3 and contribute to stabilize the transition state and lower the barrier. In the resulting intermediate m_4 (Fig. 5) a modification of the position of the expelled H_3COH molecule is observed. Here the methanol remains anchored to the glutamate residue and the OH

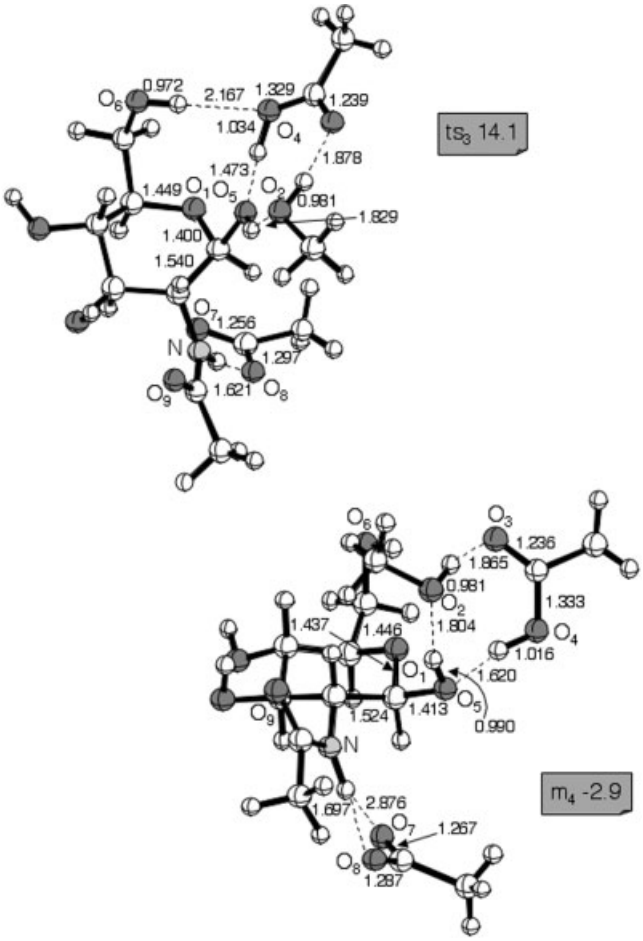

Fig. 5. Schematic representation of the structures of the critical points ts_3 and m_4 (bond lengths are in angstroms). The energy values (kcal mol^{-1}) are relative to m_1.

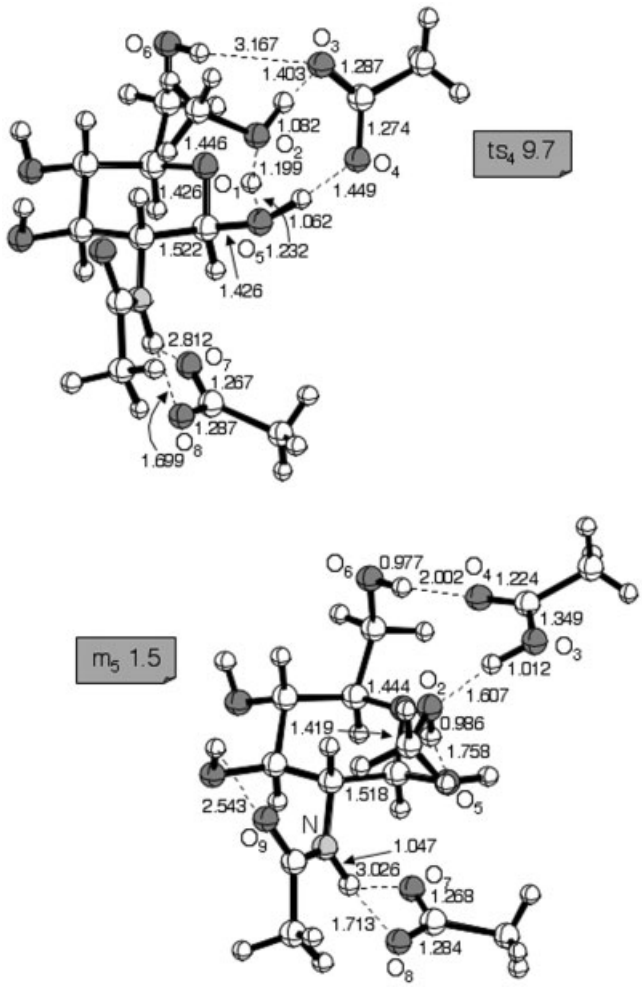

Fig. 6. Schematic representation of the structures of the critical points ts_4 and m_5 (bond lengths are in angstroms). The energy values (kcal mol^{-1}) are relative to m_1.

group at C_1 by means of two hydrogen bonds (O_5-H…O_2 and O_2-H…O_3), but its position is modified by the new orientation of the OH bond in the chair conformation.

A further aspect is interesting. After the conformational rearrangement $m_3 \rightarrow ts_3 \rightarrow m_4$, a change of the protonated oxygen of the glutamate residue could be necessary. This point is important since the protonation state found in m_4 does not necessarily correspond to that needed to start a new catalytic cycle when a new substrate and a new water molecule enter the active site. The transition structure that we have located (ts_4 in Fig. 6), shows that, to lower the activation barrier, this proton transfer does not occur directly from O_4 to O_3, but takes place within the cyclic structure of hydrogen bonds described in the previous section. Actually, the process corresponds to three simultaneous proton transfers: from O_4 to O_5, from O_5 to O_2 and from O_2 to O_3. This process results in a net proton transfer from O_4 to O_3, and requires the overcoming of an activation barrier of 12.6 kcal mol^{-1}. At the same time the glutamate residue rotates to form the hydrogen bond O_6-H…O_4. It is interesting to note that our model indicates that the leaving substrate (the methanol molecule) plays an important role in this transformation acting as a proton carrier. The resulting complex m_5 is 4.4 kcal mol^{-1} higher than m_3. Here the rotation of the glutamate residue is completed and the O_6-H…O_4 bond is well established (H…O_4 = 2.002 Å). A further point of interest concerns the structural features of m_5 that are very similar to those of the starting complex m_1. In particular the orientation of the glutamate residue is now suitable to accept a new water molecule bridging the O_6-H group and the O_4 oxygen, as found in m_1.

Mechanism 3: Ring Opening

We examine now the energy profile obtained in the investigation of mechanism 3 and reported in Figure 7. Our computations have demonstrated that the proton transfer from the Glu35 group to the endocyclic oxygen O_1 (see Scheme 3) is preceded by a rotation of this residue around the C-C bond (transition state ts_5, see Fig. 8). The rotation has the effect of moving the glutamate hydrogen closer to O_1, leading to the formation of the hydrogen bond O_1…H-O_3 that replaces the O_2…H-O_3 interaction found in the initial complex m_1. This transformation has a barrier

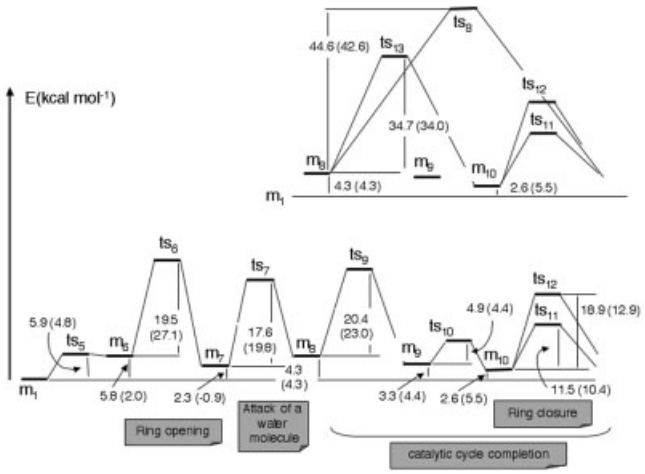

Fig. 7. Energy profiles obtained for the various steps of mechanism 3. The values in parenthesis are obtained with the solvent COSMO model.

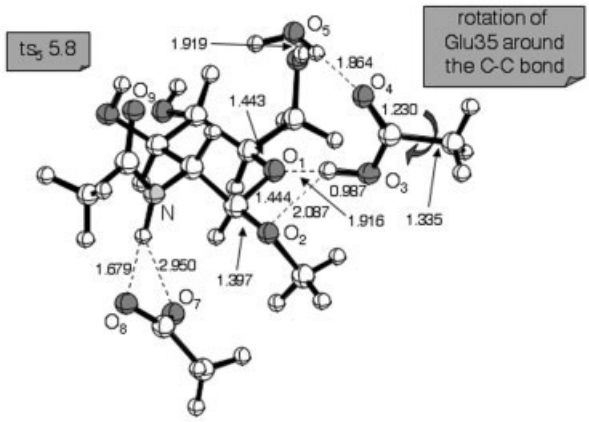

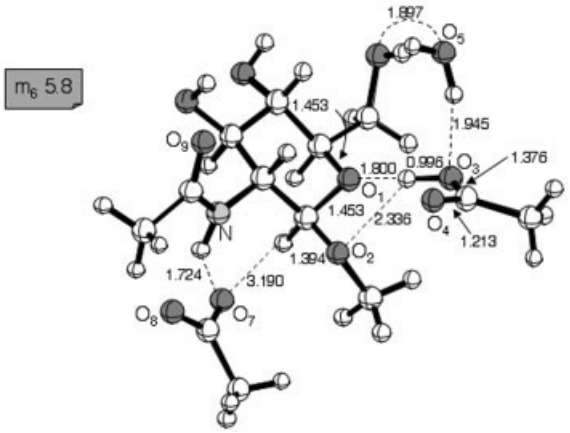

Fig. 8. Schematic representation of the structures of the critical points ts_5 and m_6 (bond lengths are in angstroms). The energy values (kcal mol^{-1}) are relative to m_1.

of 5.9 kcal mol^{-1} and the resulting intermediate m_6 is almost degenerate to the transition state. The new hydrogen bond O_1…H-O_3 in m_6 is characterized by a O_1…H distance of 1.800 Å. The subsequent reaction step is rather complicated. A proton is transferred from O_3 to O_1 and, at the same time, the Asp52 oxygen O_7 attacks the anomeric

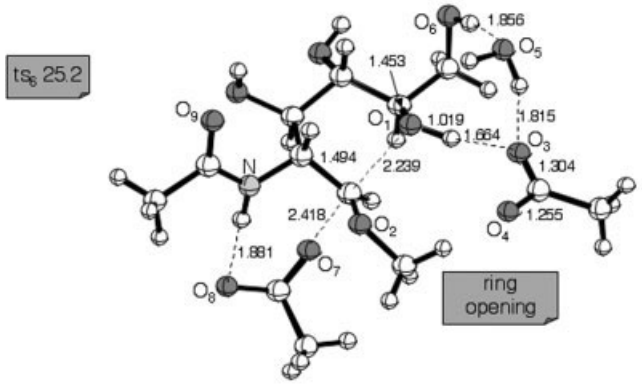

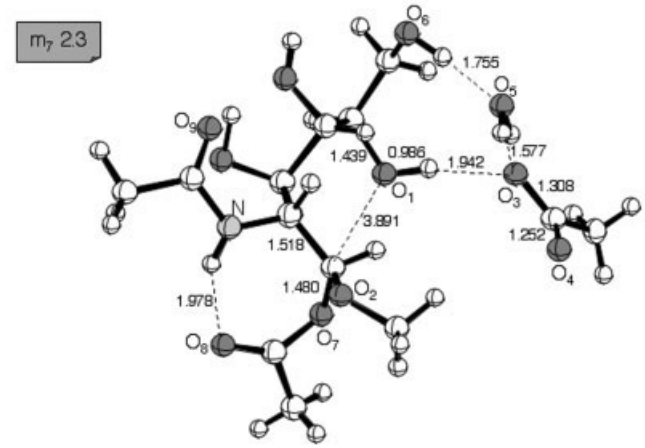

Fig. 9. Schematic representation of the structures of the critical points ts_6 and m_7 (bond lengths are in angstroms). The energy values (kcal mol^{-1}) are relative to m_1.

carbon C_1 and causes the opening of the cycle (breaking of the C_1-O_1 bond). Thus, once again, the process, which has a barrier of 19.5 kcal mol^{-1}, can be considered a S_N2-type reaction (with inversion of the anomeric configuration). The proton shift weakens the C_1-O_1 bond and catalyzes the reaction. The corresponding transition state (ts_6, see Fig. 9) resembles ts_1 of mechanism 2: the proton is almost completely transferred (O_1-H = 1.019 Å), while the O_7-C_1 and C_1-O_1 bonds (2.418 and 2.239 Å, respectively) are broken and formed approximately to the same extent. Also, as observed in ts_1, the Asp52 residue rotates around the C-C bond to move O_7 closer to C_1 and make easier the nucleophilic attack. The resulting intermediate m_7 is only 2.3 kcal mol^{-1} above m_1 (the starting Michaelis complex). Here the new C_1-O_7 bond is completed (1.480 Å) and the C_1-O_1 distance is quite large (3.891 Å), but the methanol (emulating the leaving NAG fragment) is still bonded to the anomeric carbon. It is interesting to point out that also this species (i.e. m_7) can be thought to correspond to the postulated glycosyl-enzyme intermediate of mechanism 2 where the configuration of the anomeric center C_1 has been inverted. Thus the mechanism that we are illustrating has the main features of both mechanism 2 (formation of the glycosil-enzyme intermediate) and mechanism 3 (ring opening catalyzed by the protonation of the endocy-

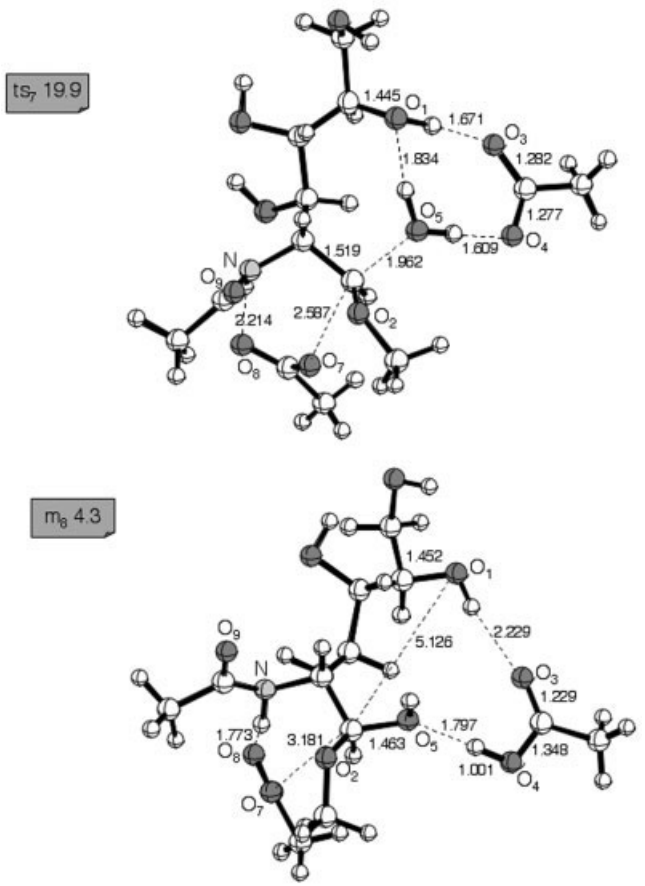

Fig. 10. Schematic representation of the structures of the critical points ts_7 and m_8 (bond lengths are in angstroms). The energy values (kcal mol^{-1}) are relative to m_1.

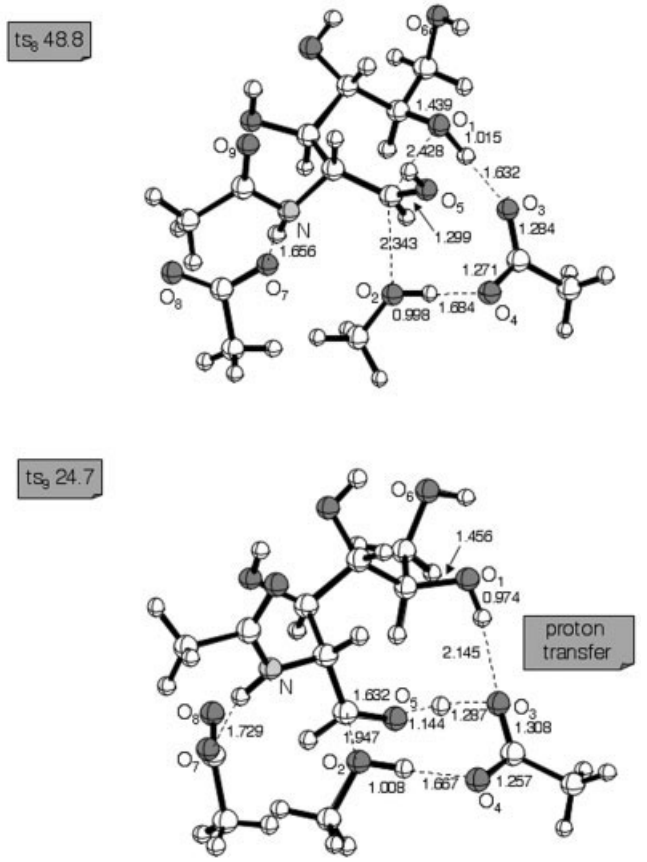

Fig. 11. Schematic representation of the structures of the critical points ts_8 and ts_9 (bond lengths are in angstroms). The energy values (kcal mol^{-1}) are relative to m_1.

clic oxygen as shown in Scheme 3). Another important aspect concerns the water molecule. This molecule has not been involved in the reaction yet and is still approximately in the initial position.

Mechanism 3: The Attack of the Water Molecule

The subsequent step ($m_7 \rightarrow ts_7 \rightarrow m_8$) is similar to the second step of mechanism 2 ($m_2 \rightarrow ts_2 \rightarrow m_3$). The water molecule acts as a nucleophile and attacks the anomeric carbon. This causes the expulsion of the Asp52 residue and a new inversion of the anomeric configuration. Thus, as observed for mechanism 2, there is a new S_N2-like process that restores the original configuration. At the same time the water transfers a proton to the glutamate residue (oxygen O_4). However, even if concerted, the two events are highly asynchronous: first the S_N2 attack and then the proton transfer. The activation barrier found for this process (transition state ts_7 in Fig. 10) is 17.6 kcal mol^{-1}. The most important components of the computed transition vector confirm the nature of ts_7. These components are the O_5-C_1 and C_1-O_7 distances (1.962 and 2.587 Å, respectively) and the H…O_4 and H…O_5 distances describing the proton transfer from O_5 to O_4.

The resulting intermediate m_8 (Fig. 10) is 4.3 kcal mol^{-1} higher than m_1. Here the new C-O_5 bond (1.463 Å) and the $O_5 \rightarrow O_4$ proton transfer are completed and two hydrogen bonds (O_4-H…O_5 and O_1-H…O_3) engage the glutamate residue and the two ends of the original ring, which are quite far away (C_1-O_1 = 5.126 Å). Thus, the final effect of the transformation $m_1 \rightarrow m_8$ is the opening of the ring and the insertion of the OH group on the original anomeric carbon C_1. This group has replaced the endocylic oxygen atom O_1 and the OCH_3 (O-NAG) group is still bonded to the anomeric center. It is evident that, to complete the catalytic cycle, we must find a way to form again the pyranose ring and to expel the OCH_3 fragment.

Mechanism 3: Ring Closure and Catalytic Cycle Completion

Different reaction channels can be followed to complete the catalytic cycle. This can take place in one single step (see the profile on the top right side of Fig. 7) through transition state ts_8 (see Fig. 11) that leads directly from the intermediate m_8 to the final product through a rather complex set of simultaneous transformations. A proton is transferred from O_1 to the glutamate oxygen O_3. At the same time another proton moves from the glutamate (O_4) to the O_2 oxygen. These two proton transfers have the effect of increasing the nucleophilic power of O_1 and that of making the OCH_3 fragment a better leaving group. The

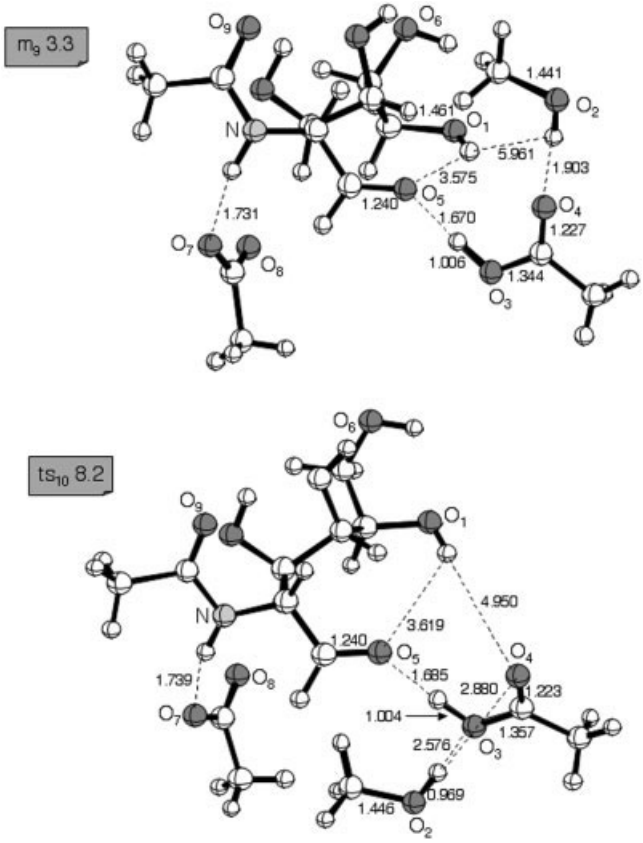

Fig. 12. Schematic representation of the structures of the critical points m_9 and ts_{10} (bond lengths are in angstroms). The energy values (kcal mol^{-1}) are relative to m_1.

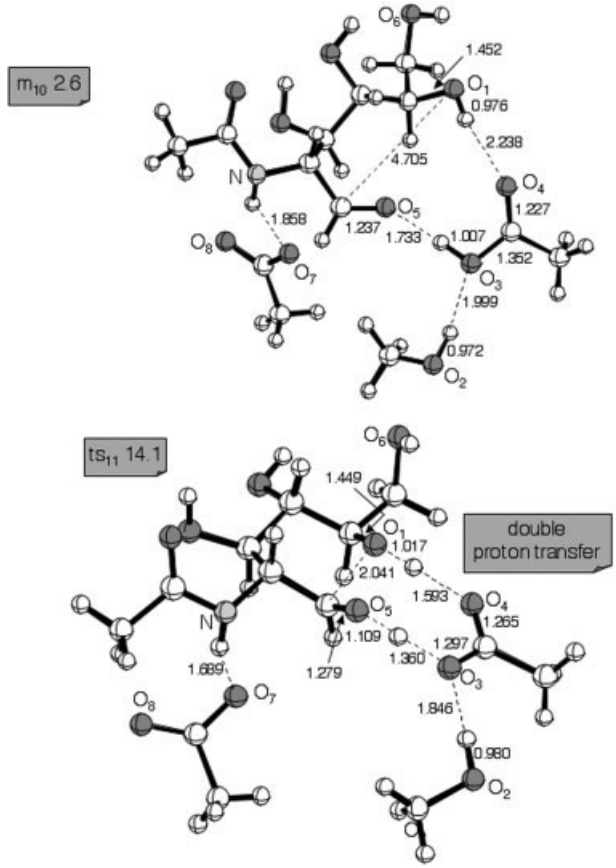

Fig. 13. Schematic representation of the structures of the critical points m_{10} and ts_{11} (bond lengths are in angstroms). The energy values (kcal mol^{-1}) are relative to m_1.

nucleophilic oxygen O_1 attacks the anomeric carbon (ring closure) and causes the expulsion of the methanol molecule. However, since a large activation barrier must be overcome (44.6 kcal mol^{-1}), this path is quite unlikely. The large barrier is probably due to the unusual value of the O_1-C_1-O_2 angle. This angle, which is expected to be close to 180° for a nucleophilic substitution, is here 141.4°. The effect is that of lowering the overlap between the HOMO of the nucleophile and the LUMO of the substrate and increasing the energy required by the transformation.

An alternative and more interesting path, with a much lower energy barrier (20.4 kcal mol^{-1}), goes through transition state ts_9 (see Fig. 11). This transition structure describes a double proton transfer (one from O_5 to O_3 and the other from O_4 to O_2) and the simultaneous breaking of the C_1-O_2 bond (1.947 Å). The final result is the release of the methanol and the formation of the C_1-O_5 carbonyl bond as shown in the resulting intermediate m_9 (Fig. 12). In m_9, which is 3.3 kcal mol^{-1} above m_1, the methanol, as observed in mechanism 2, remains anchored to the O_4 oxygen of the glutamate residue (O_2-H…O_4 hydrogen bond, H…O_4 = 1.903 Å). Also, a strong hydrogen bond between the carbonyl and the glutamate (O_3-H…O_5) contributes to stabilize m_9. In this case the hydrogen atom is almost shared between the two oxygen atoms, the O_3-H and O_5-H distances being 1.006 and 1.670 Å, respectively. An alternative and slightly more stable arrangement of the expelled methanol molecule is possible. H_3C-OH moves to the other side of the glutamate residue (transition state ts_{10} with activation barrier of 4.9 kcal mol^{-1}) and forms a hydrogen bond with the O_3 oxygen (O_2-H…O_3 hydrogen bond, H…O_3 = 1.999 Å). The resulting intermediate m_{10} (see Fig.13) is only 1.7 kcal mol^{-1} more stable than m_9. Even if the overall structural features of m_9 and m_{10} are very similar, an interesting difference must be outlined. In m_{10} the O_4 glutamate is conveniently oriented to form a hydrogen bond (O_1-H…O_4) with the O_1-H group that will be involved in the ring closure. This bond prepares a subsequent proton transfer that will occur simultaneously to the nucleophilic attack on the carbonyl group C-O_5.

It is important to point out that, since C_1 is now a pro-chiral center, the ring closure from m_{10} can follow two different paths corresponding to the attacks of the nucleophile O_1 on the two sides of the carbonyl plane. Only one, of course, leads to the correct final configuration characterized by a β C_1-OH bond. We have examined both reaction channels and we have located the corresponding transition states: ts_{11} and ts_{12} (see Figs. 13 and 14, respectively). They are both characterized by a double proton transfer: one from O_1 to O_4 (this makes O_1 a better nucleophile) and the other from O_3 to O_5. ts_{11}, which leads to the original

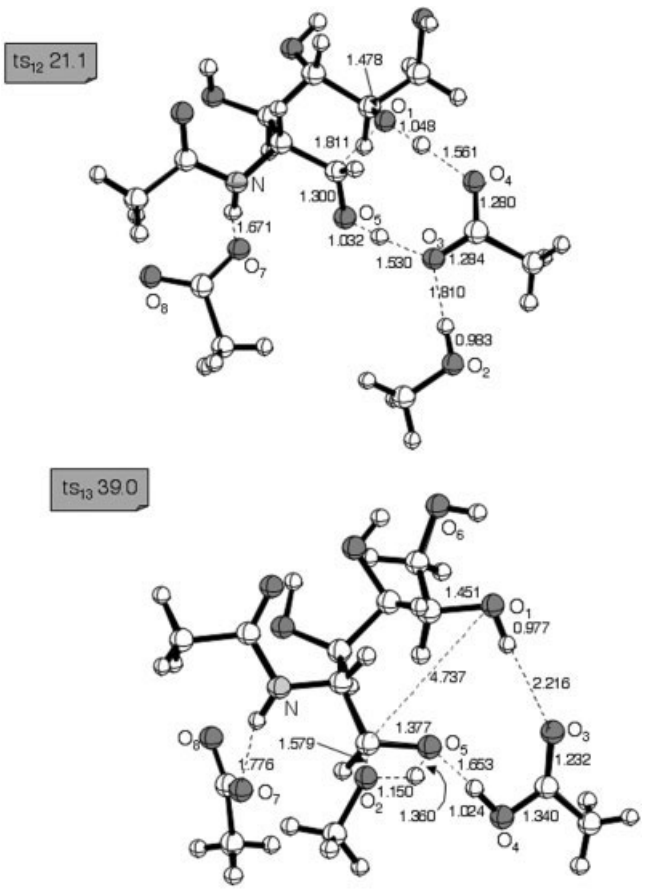

Fig. 14. Schematic representation of the structures of the critical points ts_{12} and ts_{13} (bond lengths are in angstroms). The energy values (kcal mol^{-1}) are relative to m_1.

anomeric configuration, has an activation energy of 11.5 kcal mol^{-1}, while the diastereotopic transition state ts_{12} has a significantly higher barrier (18.8 kcal mol^{-1}). Thus, since the path corresponding to ts_{12} can be ruled out on energy ground, this mechanism leads to a retention of the anomeric configuration in agreement with the experimental evidence.

The existence of a third reaction channel, originating from the intermediate m_8 and leading directly to m_{10}, has been demonstrated. The corresponding transition state ts_{13} is represented in Figure 14. However, since the activation barrier is quite large (34.7 kcal mol^{-1}), this path also is very unlikely and can be discarded.

In conclusion our results suggest that a mechanism involving a ring opening (similar to mechanism 3 of Scheme 3), exists on the potential surface. Since the higher in energy transition state involved in mechanism 3 (i.e. ts_6) is 25.3 kcal mol^{-1} above m_1 (initial complex), this mechanism, in principle, can be competitive with mechanism 2 where the higher in energy transition state (ts_2) is 23.0 kcal mol^{-1} above the Michaelis complex.

The Effect of the Protein Environment

The values of the activation energies obtained in the presence of solvent effects are reported in parenthesis in Figures 2 and 7. For mechanism 2 the barriers for the first ($m_1 \rightarrow ts_1$) and second ($m_2 \rightarrow ts_2$) step change only slightly (23.2 and 10.1 kcal mol^{-1}, respectively) and ts_2 is now 24.1 kcal mol^{-1} above m_1. For mechanism 3, a more significant variation is observed in the barrier $m_6 \rightarrow ts_6$ that becomes 27.1 kcal mol^{-1}. Thus ts_2 and ts_6 still correspond to the rate determining step along mechanism 2 and mechanism 3, respectively. However, since m_6 is stabilized by the solvent effect, ts_6 is 29.1 kcal mol^{-1} above m_1. Thus, we can suppose that in the real enzyme, mechanism 2 is favored. Less important variations are observed in the activation barriers of the subsequent steps for both mechanisms 2 and 3. An exception is found in the activation energies of the two diastereotopic transition states ts_{11} and ts_{12}. While the activation barrier only slightly decreases in the former case (10.4 kcal mol^{-1}), it becomes significantly smaller in the latter (12.9 kcal mol^{-1}). Thus, even if ts_{11} remains favored, the difference with respect to ts_{12} is only 2.5 kcal mol^{-1}.

MP2 Computations

To validate the B3LYP results we have recomputed the energy of m_1 (reactants) and that of the two main transition states ts_1 and ts_6 at the MP2 level. We have found that ts_1 and ts_6 are 27.3 and 29.2 kcal mol^{-1} higher than reactants, respectively. Even if these values are larger than the corresponding B3LYP values (22.7 and 25.3 kcal mol^{-1}, respectively), the variation is not dramatic and, more important, the relative energy of ts_1 and ts_6 does not vary significantly. This leaves unchanged the previously discussed mechanistic scenario.

CONCLUSIONS

In this paper a theoretical investigation of the catalytic mechanism of lysozyme. has been carried at the DFT level using the B3LYP functional. The most significant results can be summarized as follows:

(i) The reaction can proceed along two different paths, roughly represented as mechanism 2 and mechanism 3 in Schemes 2 and 3, respectively. Even if mechanism 2 is favored in the case of the simple model-system used here, the difference between the values of the main activation barriers found along the two paths is not too large (ts_1 and ts_6 are 22.7 and 25.3 kcal mol^{-1} higher than reactants, respectively). Thus, in principle, it is reasonable to believe that in the real enzyme the two mechanisms can become competitive.

(ii) The present results are in very good agreement with the recent experimental evidence achieved by Vocadio et al.[27] and enforce the hypothesis of a mechanism involving a glycosil-enzyme intermediate. This type of intermediate has been located both along mechanism 2 and mechanism 3. Also, the features of mechanism 3, leading to the opening of the pyranose ring, are in agreement with the data obtained by Karplus[33] by means of a molecular dynamics simulation that suggest the breaking of the endocyclic C_1-O bond.

(iii) For mechanism 2 the rate-determining step is the nuclephilic attack (S_N2-type) of one Asp52 oxygen atom at

the anomeric carbon (glycosidic bond cleavage and formation of the glycosil-enzyme intermediate). The same type of nucleophilic attack characterizes the rate determining step of mechanism 3, this time causing the breaking of the endocyclic C-O bond (ring opening) and leading again to a glycosil-enzyme intermediate. An acidic catalysis operated by the Glu35 residue has been observed in both mechanisms: a proton is transferred from the glutamic acid (Glu35) to the glycosidic oxygen in mechanism 2 or to the endocyclic oxygen in mechanism 3.

(iv) The transition states ts_1 and ts_2 (rate-determining step) along the favored mechanism (mechanism 2) are stabilized by a network of hydrogen bonds involving the C_2-bonded acetamido group and the Asp52 residue. This explains the experimental observation indicating a significant reduction of the catalytic constant after removal of the acetamido group in the substrate.

(v) The process proceeds with net retention of the anomeric configuration. In the case of mechanism 2 this is the result of a double inversion of configuration: the first occurring along the first step (glycosidic bond cleavage and formation of the glycosil-enzyme intermediate) and the second caused by the subsequent nucleophilic attack of the water. In the case of mechanism 3 the final anomeric configuration is determined by the nucleophilic attack (leading to ring closure) on the carbonyl group of the open aldehyde species. Two diastereotopic transition states have been determined in this case and that leading to the experimentally observed configuration (β C_1-OH bond) has the lower energy barrier.

(vi) The computations carried out with the inclusion of solvent effects, emulating the protein environment, do not change significantly the mechanistic scenario obtained with the gas-phase model. The most significant change is observed in the energy of ts_2 and ts_6 with respect to the initial Michaelis complex. Since the difference between the energies of these two transitions state becomes about 5 kcal mol^{-1}, mechanism 2 seems to be further favored by the protein environment.

(vii) No evidence has been found for the formation of the oxocarbenium ion that would be originated by the expulsion of the NAG unit at position E after protonation of the glycosidic oxygen (mechanism 1 of Scheme 2). It is interesting to compare these results to those obtained by Karplus and coworkers[33] in the study of the uracil-DNA glycosylase. In that case it was demonstrated that a key-interaction involving the DNA substrate phosphate groups makes possible the existence of the oxocarbenium ion intermediate. It is conceivable that, when these interaction are neglected and only the solvent dielectric effects are taken into account, the oxocarbenium ion is destabilized and the mechanism becomes concerted, as found by these authors. This is not the case for the lysozyme. Here we do not have such a type of interaction between charged groups (like phosphates) of substrate and enzyme that would be neglected in our model-system that only considers the solvent dielectric effect. The important interaction here is that between the incipient positive charge at C_1 (anomeric center) and the negatively charged Asp52 residue and this interaction leads finally to the formation of the covalent intermediate. These results suggest that a step-wise mechanism involving an oxocarbenium cation intermediate cannot be discarded a priori. Its existence can depend on particular structural features of the substrate-enzyme system and the effects of specific substrate-enzyme interactions, as pointed out in Karplus and coworkers.[33]

ACKNOWLEDGMENTS

We would like to thank C.N.R. and M.U.R.S.T. (Progetto Nazionale "Stereoselezione in Sintesi Organica: Metodologie ed Applicazioni") and Bologna University (funds for selected research topics) for the financial support of these researches.

REFERENCES

1. Sinnot ML. Catalytic mechanisms of enzymic glycosyl transfer. Chem Rev 1990;90:1171–1201.
2. McCarter JD, Withers SG. Mechanisms of enzymatic glycoside hydrolysis. Curr Opin Struct Biol 1994;4:885–892.
3. Davies G, Henrissat B. Structures and mechanisms of glycosyl hydrolases. Structure 1995;3:853–859.
4. Zechel DL, Withers SG. Glycosidase mechanisms: anatomy of a finely tuned catalyst. Acc Chem Res 2000;33:11–18.
5. Jeanloz RW, Sharon N, Flowers HM. The chemical structure of a disaccharide isolated from *Micrococcus lysodeikticus* cell wall. Biochem Biophys Res Commun 1963;13:20–25.
6. Salton MRJ, Ghuisen JM. The structure of di- and tetrasaccharides released from cell walls by lysozyme and Streptomyces F1 enzyme and the beta (1 to 4) N-acetylhexos-aminidase activity of these enzymes. Biochim Biophys Acta 1959;36:552–554.
7. Salton MRJ, Ghuisen JM. Acetylhexosamine compounds enzymically released from Micrococcus lysodeikticus cell walls. III. The structure of DI- and tetra-saccharides released from cell walls by lysozyme and Streptomyces F1 enzyme. Biochim Biophys Acta 1960;45:355–363.
8. Strynadka NCJ, James, MNG. Lysozyme revisited: crystallographic evidence for distortion of an n-acetylmuramic acid residue bound in site D. J Mol Biol 1991;220:401–424.
9. Jolles J, Jolles P, What's new in lysozyme research? Always a model system, today as yesterday. Mol Cell Biochem 1984;63:165–189.
10. Jolles J, Jauregui-Adell J, Bernier I, Jolles P. La structure chimique du lysozyme de blanc d'oeuf de poule: etude détaillee. Biochim Biophys Acta 1963;78:668–689.
11. Canfield RE. The amino acid sequence of egg white lysozyme. J Biol Chem 1963;238:2698–2707.
12. Nguyen-Huu MC, Stratmann M, Groner B, Wurtz T, Land H, Glesecke K, Sippel AE, Schutz G. Chicken lysozyme gene contains several intervening sequences. Proc Natl Acad Sci USA 1979;76:76–80.
13. Blake CCF, Koenig DF, Mair GA, North ACT, Phillips DC, Sarma VR. Structure of hen egg-white lysozyme. A three-dimensional Fourier synthesis at 2 Angstrom resolution. Nature 1965;206:757–761.
14. Blake CCF, Mair GA, North ACT, Phillips DC, Sarma VR. On the conformation of the hen egg-white lysozyme molecule. Proc Roy Soc ser B 1967;167:365–377.
15. Blake CCF, Johnson LN, Mair GA, North ACT, Phillips DC, Sarma VR. Crystallographic studies of the activity of hen egg-white lysozyme. Proc Roy Soc ser B 1967;167:378–388.
16. Phillips DC. The three-dimensional structure of an enzyme molecule Sci Am 1966;215:78–90.
17. Phillips DC. The hen egg-white lysozyme molecule. Proc Natl Acad Sci USA 1967;57:484–495.
18. Joynson MA, North ACT, Sarma V, Dickerson RE, Steinrouf LK. Low-resolution studies on the relationship between the triclinic and tetragonal forms of lysozyme. J Mol Biol 1970;50:137–142.
19. Kundrot CE, Richards FM. Crystal structure of hen egg-white lysozyme at a hydrostatic pressure of 1000 atmospheres. J Mol Biol 1987;193:157–170.

20. Moult J, Yonath A, Traub W, Smilansky A, Podjarny A, Rabinovich D, Saya, A. The structure of triclinic lysozyme at 2–5 Å resolution. J Mol Biol 1976;100:179–195.
21. Hogle J, Rao ST, Mallikarjunan M, Beddel C, McMullan RK, Sundralingam M. Studies of monoclinic hen egg white lysozyme. I. Structure solution at 4 Å resolution and molecular-packing comparisons with tetragonal and triclinic lysozymes. Acta Crystallogr sect B 1981;37:591–597.
22. Artymiuk PJ, Blake CCF, Rice DW, Wilson KS. The structures of the monoclinic and orthorhombic forms of hen egg-white lysozyme at 6 Å resolution. Acta Crystallogr sect B 1982;38:778–783.
23. Hodsdon JM, Brown GM, Sieker LC, Jensen LH. Refinement of triclinic lysozyme: I. Fourier and least-squares methods. Acta Crystallogr sect B 1990; 46:54–62.
24. Chipman DM, Sharon N. Mechanism of lysozyme action. Science 1969;165:454–465.
25. Koshland DE. Stereochemistry and mechanism of enzymatic reactions. Biol Rev 1953;28:416–436.
26. Kirby AJ, Mechanism and stereoelectronic effects in the lysozyme reaction. Crit Rev Biochem 1987;22:283–315.
27. Vocadlo DJ, Davies G J, Laine R, Withers SG. Catalysis by hen egg-white lysozyme proceeds via a covalent intermediate. Nature 2001;412:835–838.
28. Kirby AJ. The lysozyme mechanism sorted after 50 years. Nat Struct Biol 2001;8:737–739.
29. Vaney MC, Maignan S, RiesKautt M, Ducruix A. High-resolution structure (1.33 Å) of a HEW lysozyme tetragonal crystal grown in the APCF apparatus. Data and structural comparison with a crystal grown under microgravity from SpaceHab-01 mission. Acta Crystallogr D Biol Crystallogr 1996;52:505–517.
30. Lowe G, Sheppard G. Acetamido-group participation in lysozyme catalysis. Chem Commun 1968;529–530.
31. Warshel A, Levitt M. Theoretical Studies of enzymatic reactions: dielectric, electrostatic and steric stabilization of the carbonium ion in the reaction of lysozyme. J Mol Biol 1976;103:227–249.
32. Post CB, Karplus M. Does lysozyme follow the lysozyme pathway? An alternative based on dynamic, structural, and stereoelectronic considerations. J Am Chem Soc 1986;108:1317–1319.
33. Dinner AR, Blackburn GM, Karplus M. Uracyl-DNA glycosylase acts by substrate autocatalysis. Nature 2001;413:752–755.
34. Frisch MJ, Trucks GW, Schlegel HB, Scuseria EG, Robb MA, Cheeseman JR, Zakrzewski VG, Montgomery JA, Stratmann RE, Burant JC, and others. Gaussian 98, Revision A.6. Gaussian, Inc., Pittsburgh PA, 1998.
35. Becke AD. Density-functional thermochemistry. III. The role of exact exchange. J Chem Phys 1993;98:5648–5652.
36. Ziegler T. Approximate density functional theory as a practical tool in molecular energetics and dynamics. Chem Rev 1991;91:651–667.
37. Fan L, Ziegler T. Nonlocal density functional theory as a practical tool in calculations on transition states and activation energies. Applications to elementary reaction steps in organic chemistry J Am Chem Soc 1992;114:10890–10897.
38. Bottoni A, Perez Higueruelo A, Miscione GP. A DFT computational study of the bis-silylation reaction of acetylene catalyzed by palladium complexes. J Am Chem Soc 2002;124:5506–5513.
39. Bernardi F, Bottoni A, De Vivo M, Garavelli M, Keseru G, Naray-Szabo G. A hypotehetical mechanism for HIV-1 integrase catalytic action: DFW modelling of a bio-mimetic environment. Chem Phys Lett 2002;362:1–7.
40. Bottoni A, Lanza CZ, Miscione GP, Spinelli D. New model for a theoretical density functional theory investigation of the mechanism of the carbonic anhydrase: how does the internal bicarbonate rearrangement occur? J Am Chem Soc 2004;126:1542–1550.
41. Chocholousova J, Vacek J, Hobza P. Acetic acid dimer in the gas phase, nonpolar solvent, microhydrated environment, and dilute and concentrated acetic acid: ab initio quantum chemical and molecular dynamics simulations. J Phys Chem A 2003;107:3086–3092.
42. Bach RD, Thorpe C, Dmitrenko O. C-H…carboxylate oxygen hydrogen bonding in substrate activation by acyl-CoA dehydrogenase: sinergy between the H-bonds. J Phys Chem B 2002;106:4325–4335.
43. Lau EY, Newby ZE, Bruice TC. A theoretical examination of the acid-catalyzed and noncatalyzed ring-opening reaction of an oxirane by nucleophilic addition of acetate. Implications to epoxide hydrolases. J Am Chem Soc 2001;123:3350–3357.
44. DiLabio GA, Pratt DA, Wright JS. Calculation of bond dissociation energies for large molecules using locally dense basis sets. Chem Phys Lett 1998;297:181–186.
45. Wright JS, Johnson ER, DiLabio GA. Predicting the activity of phenolic antioxidants: theoretical method, analysis of substituent effects, and application to major families of antioxidants. J Am Chem Soc 2001;123:1173–1183.
46. Godbout N, Salahub DR, Andzelm J, Wimmer E. Optimization of Gaussian-type basis sets for local spin density functional calculations. Part I. Boron through neon, optimization technique and validation. Can J Chem 1992;70:560–571.
47. UniChem DGauss, Version 2.3.1. 1994; Cray Research, Inc.
48. Klamnt A. Conductor-like screening model for real solvents: a new approach to the quantitative calculation of solvation phenomena. J Phys Chem 1995;99:2224–2235.
49. Klamnt A. Calculation of UV/Vis spectra in solution. J Phys Chem 1996;100:3349–3353.
50. Turbomole, version 5.6. Institut für Physikalische Chemie und Elektrochemie Lehrstuhl für Theoretische Chemie Universität Karlsruhe Kaiserstr. 12 D-76128 Karlsruhe.
51. Barone V, Cossi M, Tomasi J. Geometry optimization of molecular structures in solution by the polarizable continuum model. J Comput Chem 1998;19:404–417.
52. Minerva T, Russo N, Sicilia E. Solvation effects on reaction profiles by the polarizable continuum model coupled with the Gaussian density functional method. J Comput Chem 1998;19:290–299.
53. Warshel A, Naray-Szabo G, Sussman F, Hwang J-K. How do serine proteases really work? Biochemistry 1989;28:3629.
54. Keeffe JR, Gronert S, Colvin ME, Tran NL. Identity proton-transfer reactions from C-H, N-H and O-H acids. An an initio, DFT, and CPCM-B3LYP aqueous solvent model study. J Am Chem Soc 2003;125:11730–11745.